Abridged version

KAWASAKI STEEL TECHNICAL REPORT
No.38 (April 1998)
Ironmaking Technology
and Tubular Products Technology

Development of a Blast Furnace Operation Simulator and its Application for Reduction of Si Content of Pig Iron

Takeshi Sato, Taihei Nouchi, Mitsuru Kiguchi

Synopsis :
A total blast furnace simulator has been developed for the planning of maintaining the best stable operation performance with inferior burden materials. The simulator has the following features: (1) Layer profile of burden materials is predicted with high accuracy. (2) Gas flow and heat transfer in the cohesive zone are modeled by focusing, with a special attention paid, on layer structure. (3) Size degradation of burden materials is modeled. The simulator has been used to precisely predict the results of operational changes for various purposes such as, [Si] reduction operation and stable operation with small size sinter. In this paper, the [Si] reduction at No. 3 blast furnace at Mizushima Works is described as a typical application of the simulator to deal with the changes of charging sequence at the bell-less top.

(c)JFE Steel Corporation, 2003

The body can be viewed from the next page.

Development of a Blast Furnace Operation Simulator and its Application for Reduction of Si Content of Pig Iron*

Takeshi Sato
Senior Researcher,
Ironmaking Lab.,
Technical Res. Labs.

Taihei Nouchi
Ironmaking Lab.,
Technical Res. Labs.

Mitsuru Kiguchi
Staff Manager,
Ironmaking
Technology Sec.,
Ironmaking Dept.,
Mizushima Works

Synopsis:

A total blast furnace simulator has been developed for the planning of maintaining the best stable operation performance with inferior burden materials. The simulator has the following features: (1) Layer profile of burden materials is predicted with high accuracy. (2) Gas flow and heat transfer in the cohesive zone are modeled by focusing, with a special attention paid, on layer structure. (3) Size degradation of burden materials is modeled. The simulator has been used to precisely predict the results of operational changes for various purposes such as, [Si] reduction operation and stable operation with small size sinter. In this paper, the [Si] reduction at No. 3 blast furnace at Mizushima Works is described as a typical application of the simulator to deal with the changes of charging sequence at the bell-less top.

1 Introduction

In the field of ironmaking, considerable effort has been made in recent years to reduce the cost of hot metal by increasing the consumption of inexpensive burden materials. As part of this trend, Kawasaki Steel has actively developed techniques for using less coking coal and pisolitic ore. On the other hand, the blast furnace is required to supply high quality hot metal, even in conventional operations, and the need to extend blast furnace life has also become greater. Thus, the establishment of a technology for stable operation with low-grade sintered ore and coke is an important problem.

In responding to such mutually incompatible requirements, it is necessary to attempt large operational changes within a short time frame. This in turn requires a more accurate operation prediction technology, which makes it possible to plan BF operation under a wide range of conditions. In consideration of these circumstances, Kawasaki Steel has developed a blast furnace operation simulator based on a two-dimensional mathematical model of the BF. This simulator is capable of evaluating the influence of changes in the burden distribution and the quality of the burden, and is used at all the company's BFs as an effective tool for predicting operational trends. This report describes the composition and features of the simulator, and presents a typical example of its use at Mizushima Works No. 3 BF to predict and analyze the effect of the large changes in burden distribution which were adopted to reduce [Si].

2 Composition of BF Operation Simulator

The blast furnace operation simulator comprises a burden distribution prediction model[1] and a two-dimensional steady model of the BF.[2,3] Combining the two models makes it possible to simulate the effect of changes in the burden distribution on the composition of the tapped pig iron, gas utilization ratio, and other operational results. It is also possible to predict temperatures in the furnace, the degree of reduction, gas composition, profile of the cohesive zone, and other operational factors, enabling a quantitative understanding of conditions in the furnace. The following sections describe the respective features of the models.

2.1 Burden Distribution Prediction Model

This numerical model has the feature of being able to simulate the following characteristic functions of the bell-less blast furnace. A flow chart of the calculations is shown in **Fig. 1**.

(1) Quantification of deviations of burden distribution in the circumferential direction as a result of switch-

* Originally published in *Kawasaki Steel Giho*, **29**(1997)1, 30-36

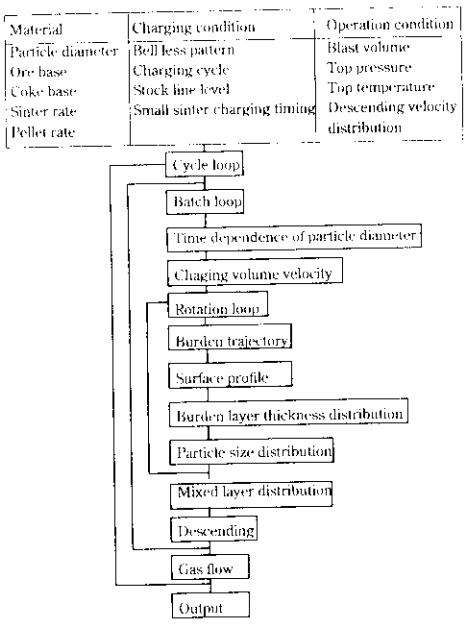

Fig. 1 Flow chart of a bell-less burden distribution model

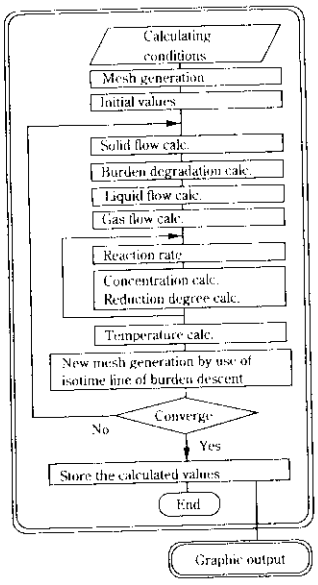

Fig. 2 Flow chart of a two-dimensional blast furnace mathematical model

ing between top bunkers (In order to calculate the deviation of burden distribution in the circumferential direction, the flow deviation behavior of material in the vertical chute is quantified based on model experiments.)

(2) Evaluation of burden distribution when using fine sintered ore

(3) Simulation of control of the amount of material discharged by the top bunker flow rate control gate

(4) Movement of particles at the distribution chute (evaluation of material throw considering the Coriolis force, gravity, friction, centrifugal force, and other factors, and simulation of the dropping trajectory)

(5) Simulation of the mixed layer profile based on calculation of ore dropping energy

(6) Evaluation of particle size segregation in each rotation, and calculation of particle size distribution in the radial direction

(7) Evaluation of the influence of gas flow on the layer profile, incorporating a two-dimensional gas flow model

(8) Simulation of the process from the top bunker outlet until laying in the furnace, making possible calculations for the charging equipment at both Chiba Works No. 6 BF and Mizushima Works No. 3 BF

With this model, it is possible to calculate the behavior of burdening and gas flow in the furnace accompanying changes in charging conditions when the tilting pattern of distribution chute is modified. Accordingly, it is also possible to determine the optimum charging pattern for a given purpose before conducting an operation experiment.

2.2 Blast Furnace Model

The blast furnace model is made up of plural submodels which correspond to various phenomena in the furnace, and makes it possible to obtain the two-dimensional distribution in the furnace in the steady condition by applying the calculation flow shown in **Fig. 2**. The composition and features of this model are described below.

(1) Generation of Mesh

The mesh used in calculations is generated as shown in **Fig. 3** so as to agree with the layer structure calculated from the solid flow model discussed below. As shown in **Fig. 4**, the upper surface and lower surface of the mesh are used to define the ore layer, and gas flow and heat transfer are then calculated in the cohesive zone. Calculations are made by direct differential method. The gas and solid flows are calculated using a triangular mesh, and the temperature and concentration, using a square mesh. Velocity is shown as a vertical flow velocity vector at each side of these figures, and the velocity potential and gas pressure are defined on a triangular circumcenter. Temperature and concentration are treated as representative values of the mesh.

(2) Solid Flow

The solid flow is treated as a potential flow, and is modeled using the equation of motion (1) and the continuation shown in Eq. (2)

$$-\mathrm{grad}\,(\phi_s) = ku_s \quad \cdots\cdots (1)$$

ϕ_s: Velocity potential (m^2/s)

k: Descent resistance of burden material

u_s: Descent velocity of burden material (m/s)

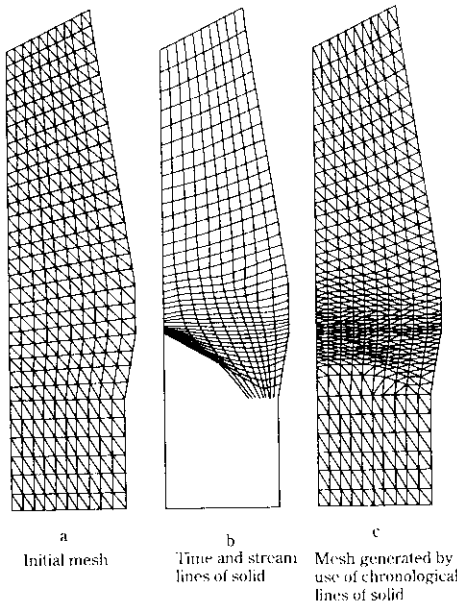

Fig. 3 Mesh generation by use of chronological lines of solid

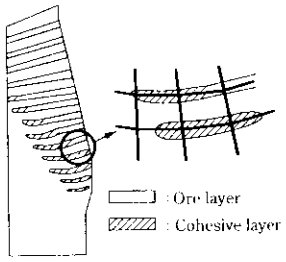

Fig. 4 Mesh formation corresponding to layer structure

$$-\mathrm{div}\,(u_s) + R_s = 0 \quad \cdots\cdots (2)$$

R_s: Source rate (s^{-1})

A quasi-stagnant zone is assumed to exist on the deadman, based on the results of experiments with a scale-model blast furnace,[4] and differing values of descent resistance, k, are used in Eq. (1) for the deadman, quasi-stagnant zone, and other zones.

(3) Burden Degradation

The reduction of particle diameter in the furnace was modeled for sintered ore based on Iwanaga's reduction pulverization equation[5] in the case of sintered ore, and on Hatano's[6] pulverization equation in the case of coke, making it possible to evaluate the influence of the RDI of sintered ore and the TI of coke on changes in particle diameter. Burden degradation is treated as the reduction in average particle size, and the number of particles after burden degradation is balanced by applying the solid flow model in combination with this model.

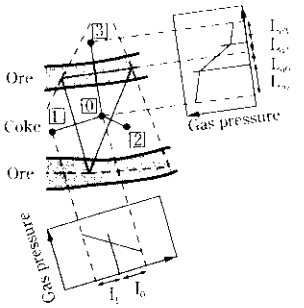

Gas flow resistance (K) between point 1 and 0 (parallel to ore layer)

$$K_1 l_0 = \frac{l_{x0} + l_{x6}}{l_{x0}/K_{x0} + l_{60}/K_{60}} l_0 + \frac{l_{x1} + l_{x6}}{l_{x1}/K_{x1} + l_{61}/K_{61}} l_1$$

Gas flow resistance (K) between point 3 and 0 (perpendicular to ore layer)

$$K_3 l_3 = K_{60} l_{60} + K_{61} l_{61} + K_{63} l_{63} + K_{63} l_{63}$$

$$l_3 = l_{x0} + l_{x6} + l_{x3} - l_{63}$$

Fig. 5 Mathematical representation of gas flow resistance parallel to and perpendicular to ore layer

(4) Liquid Flow

Many points in connection with the liquid flow in actual furnaces are unclear, and liquid flow behavior remains to be elucidated. The hypothesis used in this model assumes that the ore and the gangue content descend in parallel with the furnace profile after melting.

(5) Gas Flow

The gas flow is calculated using Ergun's equation expanded to two dimensions, as shown in Eq. (3)[7], and the continuation shown in Eq. (4).

$$-\mathrm{grad}\,(P) = KG_g \quad \cdots\cdots (3)$$

$$K = f_1 + f_2|G_g|$$

$$f_1 = 150(1-\varepsilon)^2\mu_g/(\phi d_p)^2\varepsilon^3\rho_g$$

$$f_2 = 1.75(1-\varepsilon)/(\phi d_p)\varepsilon^2\rho_g$$

P: Pressure of gas (Pa)

f_1, f_2: Ergun's resistance coefficient (s^{-1}, m^2/kg)

ε: Void factor

ϕ: Profile coefficient

d_p: Particle diameter (m)

ρ_g: Gas density (kg/m^3)

$$-\mathrm{grad}\,(G_g) + R_g = 0 \quad \cdots\cdots (4)$$

G_g: Gas mass flow velocity ($kg/m^2 \cdot s$)

R_g: Source rate ($kg/m^3 \cdot s$)

The mesh is made to agree with the layer structure in this model, as mentioned previously, and the gas flow resistance in the cohesive zone is calculated by the means shown in **Fig. 5**.

(6) Heat Transfer

The temperature distribution in the furnace is calculated from the heat balance in the square mesh shown in **Fig. 6**.

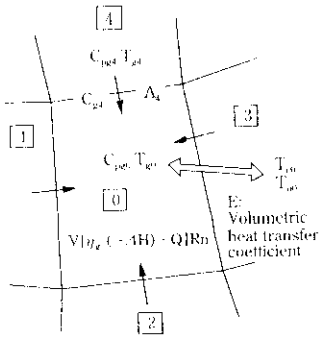

Fig. 6 Heat balance of gas phase in square mesh

$$\Sigma[A_i \,\mathrm{Max}\,(G_{gi}, 0)C_{pgi}T_{gi}] - \Sigma[A_i \,\mathrm{Max}\,(-G_g, 0)C_{pg0}T_{gi0}] + E_{gc}(T_{c0} - T_{g0}) + E_{go}(T_{o0} - T_{g0}) + V\Sigma[\eta_g(-\Delta H) + Q_{cg} + Q_{og}]R_n = 0 \cdots\cdots (5)$$

$$\mathrm{Max}\,(a, b) = a \ (a \geqq b) \\ = b \ (a < b)$$

A: Area of mesh interface (m^2)
C_p: Average specific heat (J/kg)
T: Temperature (K)
E: Heat exchange coefficient (W/K)
V: Volume of mesh (m^3)
$-\Delta H$: Reaction heat (W/m^3)
Q: Amount of sensible heat transfer from nonuniform reactions (W/m^3)
η_g: Ratio of acquisition of heat of reaction

The gas phase heat balance is shown here. The calculation is performed in the same manner for the coke and ore phases. The behavior of heat transfer between the phases differs respectively in the lumpy zone, cohesive zone, and dropping zone. The heat transfer coefficients, E, of these respective regions are shown in **Fig. 7**. For the heat transfer coefficient between particles (droplets) and gas, h_p, Ranz's equation[8] was used. The total heat transfer coefficient between the cohesive layer and gas, h_A, is expressed as shown in the following equation using the film heat transfer coefficient near the wall in stock column h_a, which was obtained by Beek,[9] and the effective heat transfer ratio λ_{co}[10] of the cohesive zone.

$$h_A = 1/(1/h_a + 0.5 \times L_o/\lambda_{eo}) \cdots\cdots (6)$$

For the heat transfer coefficient between droplets and the packed bed, h_{cm}, an equation for forced convection heat transfer[11] was used.

(7) Reactions

For the gas reduction reaction of ore, solution loss reaction, gas shift reaction, and direct reduction the total reaction velocity equations[12-14] obtained by Muchi et al. were used. The Si transfer reaction[15] considers the generation of SiO gas by the reaction between the SiO_2 in the descending slag and coke,[16] the generation of SiO gas from the coke ash in the raceway, and the absorption of Si from SiO gas to the hot metal.[17]

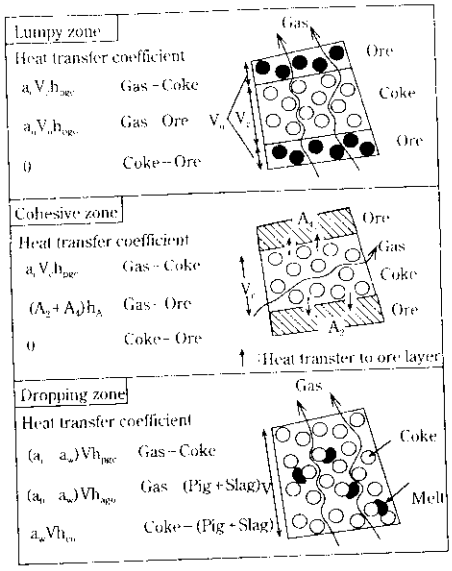

Fig. 7 Gas flow and heat exchange in each zone of blast furnace

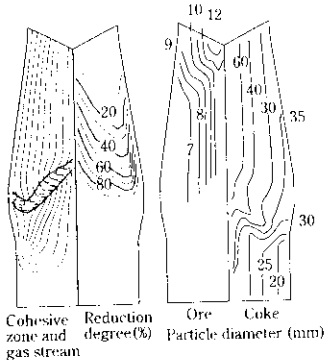

Fig. 8 Typical output of the simulator

It should be noted that, because this simulator was constructed on a work station which is connected to the company-wide network, simulation calculations for the BFs can be performed not only at the Technical Research Laboratories, where the development work was centered, but also directly from Chiba Works or Mizushima Works as a matter of course. **Figure 8** shows an example of a prediction of the cohesive zone profile, gas stream, degree of reduction, and particle diameter of the ore and coke made using this simulator.

3 Application to Actual Operation

The simulator is used in operational prediction or operational analysis when high PC ratio, high SS ratio, and similar types of operational changes are performed,

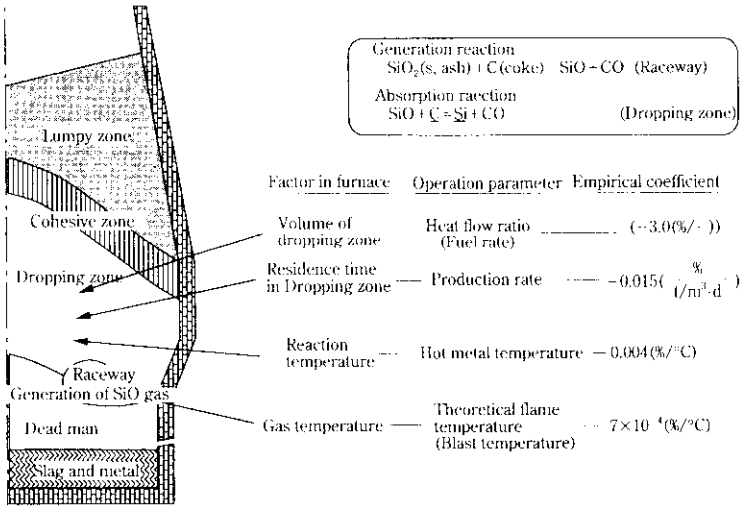

Fig. 9 Major factors influencing on [Si]

and has produced a number of positive results. In this paper, the reduction of the Si content in hot metal ([Si]) at Mizushima Works No. 3 BF will be presented as an example of a new application of the simulator to an actual operation.

3.1 Operational Factors Affecting [Si]

The SiO_2 in coke and ore can be considered to be transferred to the hot metal by the following two reactions.

· Gasification reaction

$$SiO_2(s, ash) + C(coke) = SiO + CO$$

· Absorption reaction

$$SiO + C = Si + CO$$

In the transfer of Si to the hot metal, the reaction velocity is rate governing. Therefore, the transfer of Si is controlled by the residence time (productivity) in the reaction region (dropping zone) and the temperature of the atmosphere.

The various operational parameters which influence [Si] and their influence coefficients are well known. Among them, the heat flow ratio, productivity, hot metal temperature, and theoretical flame temperature (TFT) fluctuate greatly in actual BF operation, and consequently have a large effect on [Si]. **Figure 9** shows the empirical influence coefficients of these operational parameters and the related factors in the furnace.

3.2 Comparison of Operational Parameters at Mizushima Works No. 3 and 4 BFs

Figure 10 shows the trend of [Si] at Mizushima Works No. 3 and 4 blast furnaces between January and May 1995. The [Si] level at No. 3 BF is high compared with that at No. 4 BF. **Figure 11** shows the differences in [Si] at No. 3 and No. 4 BFs by operational factor, using

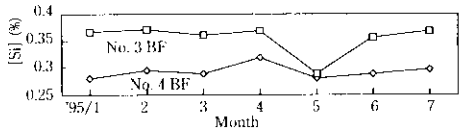

Fig. 10 Trends of [Si] at No. 3 and 4 blast furnace of Mizushima Works

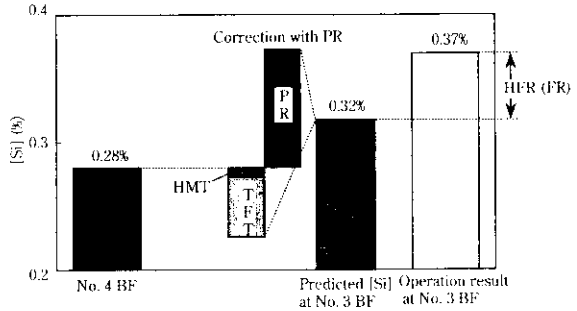

Fig. 11 Analysis of [Si] change with empirical [Si] coefficient

the above-mentioned influence coefficients. The hot metal temperature and TFT are both lower at No. 3 BF than at No. 4, and therefore are not factors in the high [Si] at No. 3. The productivity is lower at No. 3 BF and is a cause of high [Si], but a difference of approximately 0.05% still remains after this factor is taken into account. This difference is presumed to be due to the heat flow ratio, which is the remaining influence factor. Because the heat flow ratio is considered to depend mainly on the fuel rate, the trend in the fuel ratio was plotted against [Si], as shown in **Fig. 12**. From this figure, it can be understood that the high fuel rate is the cause of the high [Si], by way of the heat flow ratio.

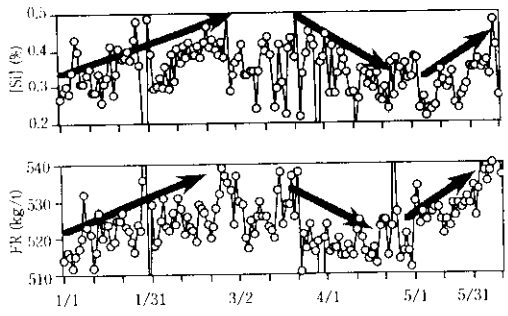

Fig. 12 Trend of [Si] and FR at No. 3 blast furnace of Mizushima Works

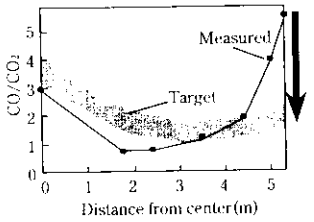

Fig. 13 CO/CO_2 distribution measured with a shaft probe and target pattern for lower [Si]

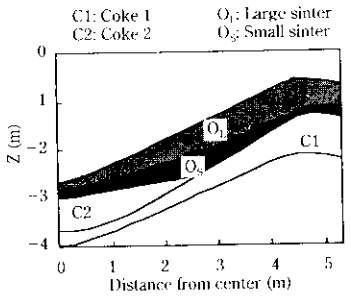

Fig. 14 Layer profile of O_SO_L charging

3.3 Factors in Low Gas Utilization Ratio at Mizushima Works No. 3 BF and Design of Burden Distribution

In order to lower the fuel rate at Mizushima Works No. 3 BF, it was indispensable to raise the gas utilization ratio (η_{co}). The results of a measurement of the CO/CO_2 distribution made with the shaft gas sampler at No 3 BF are shown in **Fig. 13**. It can be understood that CO/CO_2 was particularly high in the vicinity of the furnace wall, and it was therefore necessary to raise the gas utilization ratio in this area.

At Mizushima Works No. 3 BF, coke and ore are each divided into two lots for charging. Ore is divided into O_S and O_L by particle size, and charging is performed in the sequence C1, C2, O_S, O_L. **Figure 14** shows the layer profile in the furnace estimated by the distribution prediction model from the charging pattern in April 1995. It

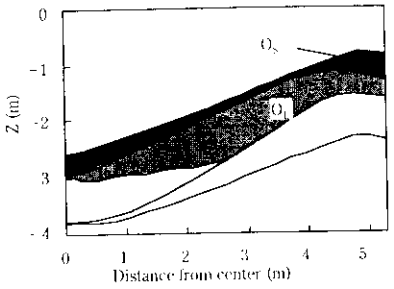

Fig. 15 Layer profile of O_LO_S charging calculated with burden distribution model

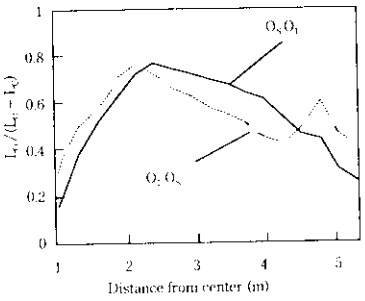

Fig. 16 Comparison of $L_O/(L_O + L_C)$ distribution for O_LO_S charging and O_SO_L charging

was estimated that, because O_S was concentrated in the intermediate area, where L_O/L_C is high, gas concentrated at the furnace wall area, reducing the gas utilization ratio at the wall. From the above, it was considered necessary to increase the gas utilization ratio at the wall by a distribution adjustment of the wall flow suppression type.

A depression is formed in the furnace intermediate area by charging C1 and C2, creating a high L_O/L_C region in this intermediate area. Charging O_S after charging C1 and C2 causes an undesirable concentration of O_S in this high L_O/L_C region. Therefore, a distribution pattern was designed to ensure stable burdening of O_S on the terrace at the furnace wall by changing the ore charging sequence to O_L, O_S in order to form a long O_L terrace, and then laying O_S on the longer terrace. The results of the distribution calculation are shown in **Figs. 15** and **16**.

3.4 Study of [Si] Reduction Effect Using Blast Furnace Simulator (Step 1)

The [Si] reduction effect of changing the charging sequence was calculated using the blast furnace simulator with the results shown in **Fig. 17**.

Before the change, O_S was concentrated in the furnace intermediate area, where L_O/L_C is high, resulting in a larger local drop in the level of the cohesive zone in that area. Conversely, it was understood that the level of the cohesive zone increased in the vicinity of the wall,

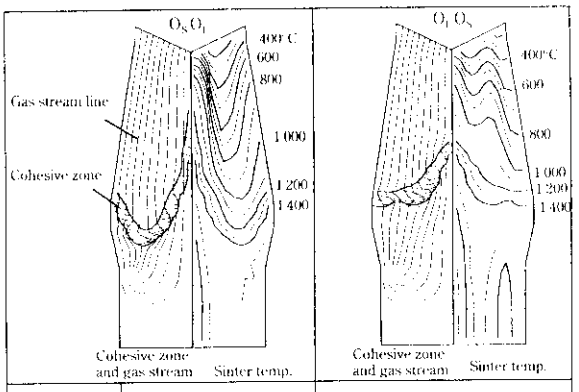

η_{CO}	(%)	45.1	46.1
TFT	(°C)	1 950	1 889
FR	(kg/t)	529	523
[Si]	(%)	0.353	0.294
Lumpy zone $\Delta P/L$	(kg/m^3)	184	189

Fig. 17 Calculated result of blast furnace simulator

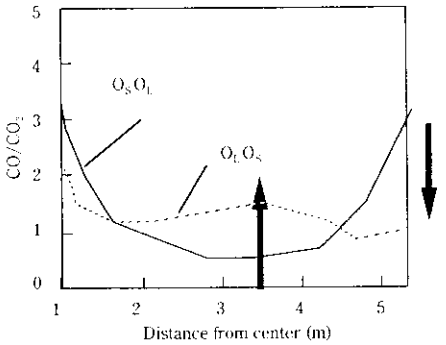

Fig. 18 Calculated result of gas distribution

and gas concentrated at the same area. After the change in the ore charging sequence described above, the cohesive zone showed a flatter layer profile, corresponding to the flattening of the O_S layer thickness. As shown in the calculated results in **Fig. 18**, the gas utilization ratio improved, particularly at the wall, and overall, gas utilization increased by approximately 1%. The amount of excess heat due to the increase in the gas utilization ratio was offset by a 60°C decrease in TFT and a 6 kg/t reduction in the fuel rate. Ultimately, a calculated result showing a 0.06% reduction in Si was obtained. However, it was predicted that suppression of the wall gas flow would cause increased pressure drop in the furnace, as shown in Fig. 17, and it was necessary to give adequate consideration to this point in the actual furnace experiments.

3.5 Study of [Si] Reduction Effect Using Blast Furnace Simulator (Step 2)

To further reduce [Si], it was considered necessary to adjust the profile of the cohesive zone. According to the

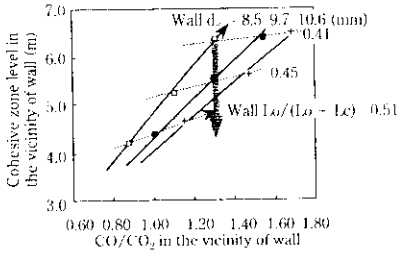

Fig. 19 Lower cohesive zone level in the vicinity of wall

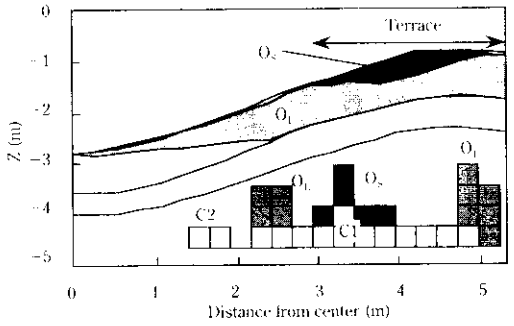

Fig. 20 Calculated result of burden distribution model for long terrace pattern

Si transfer mechanism, reducing the level of the cohesive zone in the vicinity of the furnace wall, where the concentration of SiO gas is high, can be expected to reduce [Si].

Figure 19 shows the results of a model calculation of the change in the lower cohesive zone level when $L_O/(L_O + L_C)$ in the vicinity of the wall and the particle diameter are changed. It can be understood that the lower cohesive zone level is more dependent on $L_O/(L_O + L_C)$ in the vicinity of the wall than on the particle diameter. Based on this fact, it was estimated that the lower cohesive zone level can be reduced while maintaining a specified gas flow distribution if $L_O/(L_O + L_C)$ in the vicinity of the wall is increased, assuming that permeability can be kept at the specified level by increasing the particle diameter in the vicinity of the wall by an amount corresponding to the increase in $L_O/(L_O + L_C)$. A calculation was made with the burden distribution model, with the results shown in **Fig. 20**. Forming a depression by greatly extending the O_L terrace makes it possible to reduce L_{OS}/L_{OL} in the vicinity of the furnace wall while suppressing the inflow of O_S to the center. At the same time, changing the coke pattern so as to increase L_O/L_C at the wall makes it possible to maintain the wall gas flow.

3.6 Results of Experiment with Actual Furnace

Based on the results of the prediction calculations made with the burden distribution model and blast furnace simulator in the previous section, an operational

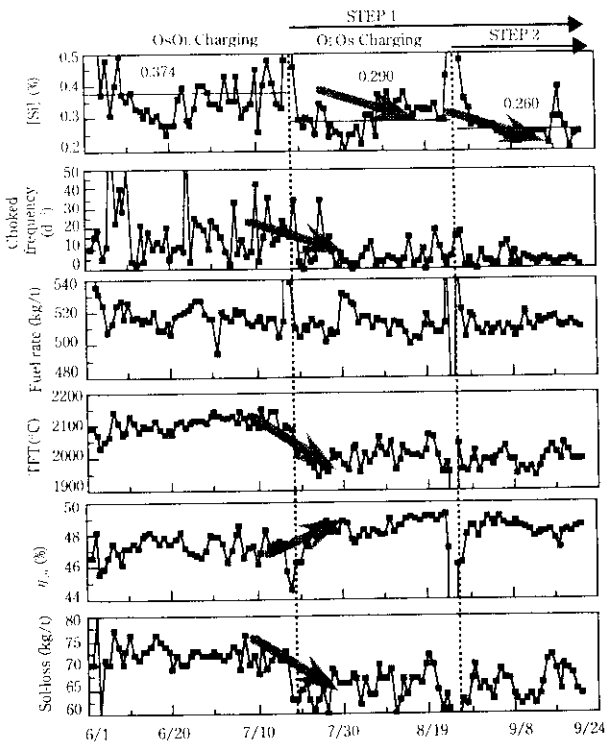

Fig. 21 Operation results of Mizushima Works No. 3 blast furnace

experiment was carried out at Mizushima Works No. 3 BF. The trend in the operation is shown in **Fig. 21**.

As calculated with the model, the change in the charging sequence resulted in an increase of approximately 1% in η_{co} and a decrease of 0.08% in [Si] (Step 1). The results measured with the shaft gas sampler before and after the change in the charging sequence (Step 1), as shown in **Fig. 22**, were also the same as the estimates made with the model, showing an increase in the gas utilization ratio at the wall and flattening of the gas distribution. **Figure 23** shows the relationship of TFT and [Si] with the changed charging sequence (Step 1), together with a straight line having the inclination of the correlation coefficient. This figure shows that it has become possible to reduce TFT by approximately 100°C by increasing the gas utilization ratio, and that it is now possible to suppress the generation of SiO gas and reduce [Si]. Moreover, a further reduction of 0.03% in [Si] was observed, with TFT and η_{co} remaining at the specified levels, when distribution was controlled so that O_S was placed toward the furnace center and O_L was placed toward the wall (Step 2).

4 Conclusion

A blast furnace operation simulator was developed as a high-accuracy operation prediction tool. The simulator was applied to operation planning for [Si] reduction at

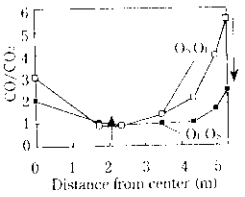

Fig. 22 Comparison of gas utilization distribution

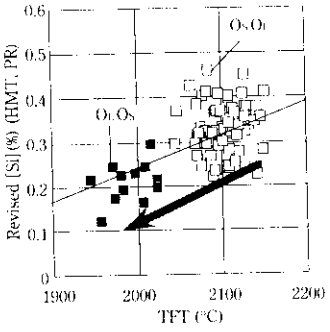

Fig. 23 Relationship between TFT and corrected [Si]

Mizushima Works No. 3 blast furnace, where it was used to predict and analyze the effect of changes in the burden distribution, and is now used as a practical method of operation planning and analysis at all the blast furnaces of Kawasaki Steel.

References

1) T. Nouchi, T. Sato, S. Miyagawa, K. Takeda, and H. Itaya: *CAMP-ISIJ*, **7**(1994), 1004
2) Y. Sawa, K. Takeda, and S. Taguchi: Proc. 50th Iron making Conf. of AIME, **50**(1991), 417
3) T. Sato, H. Matsubara, K. Takeda, H. Itaya, and H. Nishimura: *CAMP-ISIJ*, **8**(1995), 140
4) T. Sato, S. Miyagawa, and H. Itaya: *CAMP-ISIJ*, **6**(1993), 887
5) Y. Iwanaga: *Tetsu-to-Hagané*, **68**(1982), 740
6) M. Hatano, T. Miyazaki, and Y. Iwanaga: *Tetsu-to-Hagané*, **65**(1979), 1365
7) S. Ergun: *Chem. Eng. Progr.*, **48**(1952), 59
8) W. E. Ranz: *Chem. Eng. Progr.*, **48**(1952), 247
9) J. Beek: *Advances in Chem. Eng.*, **13**(1962), 203
10) T. Sugiyama, Y. Sato, M. Nakamura, and Y. Hara: *Tetsu-to-Hagané*, **65**(1979), s532
11) W. H Giedt: *Principles of Engineering Heat Transfer*, (1957), 146
12) I. Muchi, J. Yagi, K. Tamura, and A. Moriyama: *J. Jpn. Inst. Met.*, **30**(1966), 826
13) J. Yagi, H. Nishio, K. Sasaki, and I. Muchi: *J. Jpn. Inst. Met.*, **31**(1967), 711
14) J. Yagi and I. Muchi: *J. Jpn. Inst. Met.*, **32**(1968), 1316
15) M. Sumito: *Tetsu-to-Hagané*, **66**(1980), s66
16) N. Tsuchiya, M. Tokuda, and M. Otani: *Tetsu-to-Hagané*, **58**(1972), 1927
17) S. Taguchi, N. Tsuchiya, H. Kubo, K. Ichihuji, and K. Okabe: *Tetsu-to-Hagané*, **68**(1982), 2311